Published in final edited form as:

J Phys Chem B. 2016 February 4; 120(4): 715–723. doi:10.1021/acs.jpcb.5b12339.

Fluorescein: a Photo-CIDNP Sensitizer Enabling Hyper-Sensitive NMR Data Collection in Liquids at Low Micromolar Concentration

Yusuke Okuno and **Silvia Cavagnero**

Department of Chemistry, University of Wisconsin - Madison, 1101 University Ave., Madison, Wisconsin, 53706, USA

Abstract

Photochemically induced dynamic nuclear polarization (photo-CIDNP) is a powerful approach for sensitivity enhancement in NMR spectroscopy. In liquids, inter-molecular photo-CIDNP depends on the transient bimolecular reaction between photoexcited dye and sample of interest. Hence the extent of polarization is sample-concentration dependent. This study introduces fluorescein (FL) as a photo-CIDNP dye whose performance is exquisitely tailored to data collection at extremely low sample concentrations. The photo-CIDNP resonance intensities of tryptophan in the presence of either FL or FMN (i.e., the routinely employed flavin mononucleotide photosensitizer) in the liquid state show that FL yields superior sensitivity and enables rapid data collection down to an unprecedented 1 micromolar concentration. This result was achieved on a conventional spectrometer operating at 14.1 Tesla, and equipped with a room-temperature probe (i.e., non-cryogenic). Kinetic simulations show that the excellent behavior of FL arises from its long excited-state triplet lifetime and superior photostability relative to conventional photo-CIDNP sensitizers.

Keywords

photo-CIDNP; NMR; sensitivity enhancement; fluorescein; photochemistry; nuclear hyperpolarization

Liquid-state nuclear magnetic resonance (NMR) spectroscopy is a prime tool to investigate molecular structure and dynamics at atomic resolution under non-perturbative conditions. NMR structural studies typically encompass a wide array of molecules, ranging from the fields of material science and organic chemistry to structural biology[1–4]. Unfortunately, the low intrinsic sensitivity of NMR spectroscopy imposes severe limitations to the number of detectable nuclear spins, and typical liquid-state samples are in the high-micromolar to millimolar concentration regime. Over the last few decades, a number of advances contributed to mitigate the low sensitivity of NMR spectroscopy. These include high applied

Correspondence should be addressed to S.C. (; Email: cavagnero@chem.wisc.edu, Phone: 608-262-5430)

Supporting Information

Supporting text and figures including additional details on kinetic simulations, effect of laser irradiation time, FL-mediated photo-CIDNP in the presence of different amino acids, and photodegradative processes. This information is found on the internet at http://pubs.acs.org.

fields, pulsed Fourier-transform techniques and cryogenic probes. More recent approaches focused on generating hyperpolarization by transiently shifting the Boltzmann distribution of nuclear spin states[5–7]. These strategies include dissolution dynamic nuclear polarization (DNP)[8], para-hydrogen-induced polarization (PHIP) coupled with signal amplification by reversible exchange (SABRE)[9–11], optical pumping[12,13], methods relying on the Haupt effect[14], Overhauser dynamic nuclear polarization (DNP)[15] and photo-chemically induced dynamic nuclear polarization (photo-CIDNP)[16,17]. Given its short hyperpolarization time (~10^{-6} s) and highly non-perturbative nature, photo-CIDNP has recently received considerable attention as a hyperpolarization tool for aromatic amino acids, polypeptides and proteins in solution[7,18–24].

Nuclear spin hyperpolarization by photo-CIDNP in liquids is governed by the radical pair mechanism[16,25,26], which involves a reversible electron transfer between the molecule of interest and a photo-excited triplet state photosensitizer in the context of a transient triplet ion pair.

Although photo-CIDNP in the solid state, which typically proceeds via a different mechanism[18,27], has previously reached low concentrations down to ~100 nM[28], photo-CIDNP studies in solution have not pushed the low-concentration limit to date. As a result, typically photo-CIDNP studies in liquids employ ~1 mM or higher sample concentration[26,29,30]. Recent developments by Cavagnero and coworkers enabled photo-CIDNP data collection at 5 μM in the presence of catalytic amounts of oxygen-scavenging and reducing enzymes[22]. However, overall, there is still an unfulfilled critical need for efficient data collection at even lower concentrations, in liquid-state nuclear magnetic resonance.

In this work, we introduce the photo-CIDNP sensitizer dye fluorescein, primarily active in its dianion form (FL), and we show that its photophysical properties are exquisitely tailored to photo-CIDNP data collection at low sample concentrations. We demonstrate that efficient data collection down to 1 μM sample concentration can be achieved on a commercially available narrow-bore 14.1 Tesla (600 MHz) NMR spectrometer equipped with a room-temperature probe and adapted to accommodate laser-enhanced data collection.

Previous usage of the FL dye in the context of photo-CIDNP was limited. The only reported studies were performed at low field (2.1 Tesla, i.e., 90 MHz) and at high sample concentration[31,32] (10–100 mM).

Experimental Methods

Amino acids and photo-sensitizers

^{13}C-^{15}N-labeled Trp was purchased from Sigma-Aldrich (574597) or from Cambridge Isotopes (CNLM 2475-H-0.1). ^{13}C-^{15}N-labeled Tyr (607991) and His (608009) were purchased from Sigma-Aldrich. The photo-CIDNP sensitizers flavin mononucleotide (FMN, F8399) and fluorescein (FL, F6377) were purchased from Sigma-Aldrich.

Oxygen-scavenging enzymes

The enzymes glucose oxidase (GO, from *Aspergillus niger*, catalog number G7141, Enzyme Commission classification code: EC 1.1.3.4) and catalase (CAT, from bovine liver, catalog number C40, EC 1.11.1.6) were purchased from Sigma-Aldrich (St. Louis, MO), and nitrate reductase (NR, from Arabidopsis thaliana, catalog number AtNaR, EC 1.7.1.1) was acquired from NECi (Lake Linden, MI). All enzymes, provided in freeze-dried form, were separately dissolved in 30 mM potassium phosphate (pH 7.0). Separate single-use GO and CAT stock solutions (ca. 5.5 −6.2 and 4.2–5.2 μM, respectively) were prepared and stored at −80 °C after flash-freezing in liquid nitrogen. The concentration of GO and CAT were measured using extinction coefficients of 267,200 $M^{-1}cm^{-1}$ at 280 nm[33] and 912,500 $M^{-1}cm^{-1}$ at 276 nm[33], respectively. The activity of GO and CAT was found to vary significantly from batch to batch. The specific activities of GO and CAT batches used in this work were 100,000–250,000 units/mg and 2,000–5,000 units/mg, respectively. One unit of GO is defined as the amount of enzyme able to oxidize 1.0 μmole of β-D-glucose to D-gluconic acid and H_2O_2 per minute at pH 5.1 at 35 °C. One unit of CAT is defined as the amount of enzyme required to decompose 1.0 μmole of H_2O_2 per minute at pH 7.0 at 25 °C. When relevant, the NR enzyme was also used. 10 units/mL NR stock solution was used. One unit is defined as the amount of enzyme that reduces 1.0 μmole of nitrate to nitrite per min at pH 7.5 and 30 °C, with NADH serving as the substrate. Enzyme aliquots were thawed in a water bath at room temperature before use.

NMR sample preparation

All NMR samples contained 5–10 % D_2O and 10 mM potassium phosphate (pH 7.0 ± 0.1). The photo-CIDNP experiment in the presence of the GO and CAT enzymes included 5 mM D-glucose (158968, Sigma-Aldrich), and 0.24–54 μM and 0.15–0.30 μM of GO and CAT, respectively. The enzyme concentrations were adjusted to provide optimal photo-CIDNP intensities on a reference sample containing 20 μM Trp every time new enzyme stocks were made. When relevant, 0.3 units per 700 μL of NR was used in experiments employing the FMN sensitizer, where the full NR-GO-CAT tri-enzyme system was used[22]. All the samples used for photo-CIDNP experiments were incubated in the NMR spectrometer for at least 15 min for the oxygen concentration to reach a steady state.

Photo-CIDNP NMR experiments

All photo-CIDNP NMR experiments were carried out with an argon ion laser (2017-AR, Spectra-Physics-Newport Corporation, Irvine, CA) in multiline mode (main lines at 488 and 514 nm). The laser light was focused into an optical fiber using a convex lens (LB4330, Thorlabs, Newton, NJ) and a fiber-coupler (F-91-C1-T, Newport Corporation). The optical fiber was guided into a glass NMR-tube coaxial insert (WGS-5BL, Wilmad-Labglass, Buena, NJ), which was then inserted into the NMR tube and adjusted to be 5mm above the receiver coil region. The nominal laser power was assessed with a power meter prior to the NMR experiments, at the optical fiber tip to be inserted in the NMR tube. A 1D version of the ^{13}C-PRINT pulse sequence[23] (with ^{13}C chemical-shift evolution time set to zero) was used for all photo-CIDNP experiments, unless otherwise stated. The experiment was run in constant-time mode, with the total evolution time in the indirect dimension set to 13 and 27

ms for side-chain and C^{α} carbons, respectively. The spectral width was set to 9,000 Hz with 2,700 complex points. Unless otherwise stated, all photo-CIDNP data were collected at 25 °C on a Varian INOVA 600 MHz (14.1 Tesla) NMR spectrometer equipped with a triple-resonance $^{1}H\{^{13}C,^{15}N\}$ triple-axis gradient room-temperature (i.e., not cryogenic) probe. Laser irradiation time was set to 0.1 s. This value was chosen after performing sample experiment testing the S/N dependence of laser irradiation time (Fig. S1). The relaxation delay was set to 10 s and 2.5 s for all single-scan and the other experiments, respectively. All 1D time-domain data were apodized with a 5 Hz exponential line-broadening function and baseline corrected with a multi-point baseline routine using the Mesternova Software (v. 10.0, Mestrelab Research, SL, Santiago de Compostela, Spain).

Non-laser-assisted reference NMR experiments

Higher-field non-laser-enhanced NMR experiments were performed on a 900 MHz (21.2 Tesla) Agilent NMR spectrometer (Direct Drive2 900 console) equipped with a 5 mm $^{1}H\{^{13}C^{15}N\}$ cryogenic probe. All NMR samples contained 5 % D_2O and 10mM potassium phosphate (pH 7.0). No GO-CAT enzymes nor D-glucose were added to the samples. All measurements were performed at 25 °C.

Determination of S/N and cumulative S/N

The signal-to-noise ratio (S/N) was determined according to

$$S/N=2.5\times\frac{S}{N_{PTP}}, \quad (1)$$

where S denotes the NMR signal, i.e., the resonance intensity riding above the noise envelope., and N_{PTP} denotes the peak-to-peak noise amplitude. The latter was evaluated within the 6–7 and 8–9 ppm ranges for aromatic resonances, and from the 2.0–3.5 ppm range for aliphatic resonances. The cumulative S/N was evaluated as

$$S/N=2.5\times\frac{\sum_{k=1}^{n}S_k}{\sqrt{\sum_{k=1}^{n}(N_{PTP})_k^2}}, \quad (2)$$

where n denotes the number of transients, S_k denotes the signal intensity of interest, and $N_{PTP,k}$ denotes the peak-to-peak noise amplitude of the k^{th} experiment.

Electronic absorption spectroscopy

Electronic absorption data were collected with a Hewlett-Packard 8452A diode-array spectrophotometer. Unless otherwise stated, samples were removed from the NMR tube after NMR data collection, thoroughly mixed and transferred to a disposable cuvette (14–878, Fisher Scientific, Pittsburgh, PA) for electronic absorption data collection. Some absorption spectra were also recorded directly in the NMR tube as described[22]. Briefly, the NMR tube containing the sample of interest was inserted in a disposable cuvette (14–955, Fisher Scientific, Pittsburgh, PA) and secured to the bottom of the cuvette via a glued NMR

cap. The interstitial space between the cuvette and the NMR tube was then filled with water[22].

Trp fluorescence emission spectroscopy

All Trp fluorescence emission data were collected at 25 °C on a PC1 fluorimeter (ISS, Urbana Champaign, IL) upon excitation at 280 nm. Quartz cuvette (Hellma GmbH & Co. KG, Müllheim, Germany) was used, and slit widths of both excitation and emission channels were set to 0.5 mm, corresponding to a 4 nm bandwidth.

Kinetic Simulations

The procedures followed for the kinetic simulations carried out in this work are described in the Supporting Information.

Results and Discussion

FL is an effective photo-CIDNP sensitizer in the presence of catalytic amounts of glucose oxidase and catalase

The structures of FL and typical photo-CIDNP dye flavin mononucleotide (FMN) are shown in Figure 1. Previous studies[22] showed that photo-CIDNP significantly decreases in the presence of molecular oxygen. This phenomenon is likely due to the quenching of the photoexcited triplet dye by ground-state oxygen ($^3O_2$) and substrate photodegradation by the resulting singlet oxygen ($^1O_2$). Hence, we minimized the deleterious effect of O_2 upon addition of catalytic amounts of the glucose oxidase (GO) and catalase (CAT) enzymes to NMR samples as described[22]. This operation was further justified by the explicit report that molecular oxygen quenches the photoexcited T_1 triplet state of FL[12,34], the photo-sensitizer analyzed in this work. As expected, the 1D ^{13}C PRINT photo-CIDNP NMR spectrum of Trp in the presence of FL (under laser-on, i.e., *light* conditions) yields higher S/N in the presence of catalytic amounts of the GO-CAT enzymes (Fig. 1c).

FL is a more effective photo-CIDNP sensitizer than FMN, at low Trp concentration

Next, we established an explicit comparison between the Trp concentration dependence of photo-CIDNP in the presence of optimized amounts of either the FMN or FL dyes. Single-scan 1D ^{13}C PRINT photo-CIDNP[23] data were collected and the results are reported in panels a and b of Figure 2. At high Trp concentration, close to the millimolar range, FMN is a better photosensitizer than FL. However, as the Trp concentration approaches 100 μM or lower, FL outperforms FMN. This result is best appreciated by noting that the low concentration range yields ratios of signal-to-noise (S/N) values > 1, as shown in panel b of Figure 2. It is worth noting that under our experimental conditions FMN yields a S/N of zero at ≤ 5 μM Trp concentration, corresponding to no detectable signal. However, a good-quality spectrum is obtained in the presence of FL. Clearly, FL is a much better photo-CIDNP sensitizer than FMN at low Trp concentration. In all, the above data show that FL is particularly well suited to the analysis of low-concentration NMR samples, enabling NMR data collection at unprecedented sensitivity.

Remarkably, a comparison between the S/N achieved with the 1D ^{13}C PRINT photo-CIDNP pulse sequence experiments for the $^{13}C^{\eta 2}$-^{1}H Trp side-chain and the $^{13}C^{\alpha}$-^{1}H Trp backbone resonances at 14.1 Tesla (i.e., with a 600 MHz spectrometer) shows good S/N, at the very low 5 μM Trp concentration (Fig. 2c).

An additional evaluation of the excellent nature of the enhancement is provided by a reference sensitivity enhanced HSQC experiment (^{1}H-^{13}C SE-HSQC[16]) performed on an identical sample at the higher field of 21.2 Tesla (i.e., on a 900 MHz spectrometer) on a magnet equipped with a cryogenic triple-resonance probe. This experiment yielded no signal (Fig. 2c). A comparison between the 14.1 and 21.2 Tesla experiments shows that remarkable sensitivity can be rapidly achieved via ^{1}H-^{13}C photo-CIDNP in the presence of FL even on a routinely available NMR spectrometer.

Long-term data collection is feasible

Next, we show that FL yields excellent results upon long-term data collection. As shown in Figure 3, 300 consecutive photo-CIDNP scans were successfully collected on the same sample in the presence of either FL or FMN. We also acquired laser-off reference data consisting of a sensitivity-enhanced ^{1}H-^{13}C HSQC (SE-HSQC) experiment[35]. An enhancement factor up to 21-fold was obtained for 1D ^{13}C PRINT relative to SE-HSQC, and over 300 scans could be acquired with only moderate signal losses due to photodegradation.

Both Tyrosine (Tyr) and Trp undergo effective photo-CIDNP at low micromolar concentration in the presence of FL

To investigate whether FL may be an effective photo-CIDNP sensitizer for amino acids other than Trp, we tested two other residues known to undergo ^{13}C photo-CIDNP, Tyr and histidine (His), in the presence of FL at 5 μM concentration. Interestingly, Tyr exhibits substantial S/N enhancement upon laser irradiation (light conditions) relative to laser-off data collection (dark conditions), as shown in Figure S2. No significant photo-CIDNP enhancement was observed in the case of His (Fig. S2). The reasons behind the lack of photo-CIDNP responsiveness exhibited by the latter amino acid are presently unknown and beyond the scope of this study. The excellent results exhibited in the presence of Trp and Tyr highlight the potential usefulness of the FL photosensitizer for the selective detection of Trp and Tyr at low micromolar concentration in biologically relevant systems.

Photo-CIDNP measurements can be extended down to 1 micromolar Trp concentration

Encouraged by this result, we proceeded to examine photo-CIDNP at the extremely low Trp concentration of 1 μM in the presence of an optimized total concentration of FL (2.4 μM) and the oxygen-scavenging GO-CAT enzymes, at 14.1 Tesla. While single-scan experiments did not yield a particularly large S/N, a moderate degree of signal averaging (8 scans) was carried out, so that a better S/N could be obtained while minimizing photodegradative processes (Fig. 4). Under these conditions we could rapidly achieve good sensitivity in only a few seconds. The photo-CIDNP enhancement is extremely high, though not directly quantifiable due to the lack of measureable signal in the corresponding dark (i.e. laser-off) experiment. A reference non-laser-assisted SE-HSQC experiment, carried out on an equivalent 1 μM Trp sample with a $\{^{1}H,^{13}C,^{15}N\}$ cryogenic triple-resonance probe at 21.2

Tesla, (i.e., one of the highest presently available fields for NMR data collection), yielded no signal (Fig, 4a). Interestingly, in order to achieve a comparable S/N in the absence of laser-assisted technology, we had to resort to data collection at 21.2 Tesla for 15,872 scans (Fig. 4b). Hence our photo-CIDNP setup in the presence of FL enables efficient data collection at 1 μM concentration, with a time saving of more than 1,980-fold over data collection with state-of-the-art high-field instrumentation equipped with a cryogenic probe.

Kinetic simulations provide insights into the origin of FL effectiveness of as a photo-CIDNP sensitizer

In order to gain additional insights into the origin of FL's effectiveness as a photo-CIDNP sensitizer we carried out kinetic simulations according to the reaction scheme of Figure 5a. The corresponding energy diagram, listing the main relevant kinetic steps, is shown in Figure 5b. In all simulations, we focused on evaluating the triplet-state concentration of the photo-CIDNP dye ($[^{T1}D]$) upon continuous laser light irradiation. Given that we observed that dye concentration needs to be optimized for each photo-CIDNP experiment at any given laser power/irradiation time/total Trp concentration, we decided to probe the effect of overall dye concentration ($[D]_{tot}$) on the photoexcited triplet-state dye under steady-state conditions. Steady-state was reached after about 10 ms, i.e., much earlier than the experimental laser irradiation time of 0.1 s (Fig. S3), thereby supporting that steady-state conditions have fully been achieved in all experiments presented here. First, we considered the limiting behavior of the photo-CIDNP dye at very low total Trp concentration, by setting $[Trp]_{TOT} \rightarrow 0$. This condition corresponds to neglecting all kinetic steps involving Trp in the kinetic scheme of Figure 5a. A Jablonski-type energy diagram is also shown in Figure 5b. As shown in Figure 5c, a very high concentration of the triplet-state dye ^{T1}D is computationally predicted, in case the intermolecular processes depopulating ^{T1}D (including dye-to-dye intermolecular collisions) and light absorption by the dye throughout the length of the NMR sample are neglected. This scenario is illustrated in the solid line of Figure 5c. On the other hand, when dye-to-dye intermolecular collisions are included in the calculations (short-dashed line of Fig. 5c), strong deviations from the idealized curve are present. When both dye-to-dye collisions and light penetration throughout the NMR sample are taken into account, the ^{T1}D concentration is predicted to decrease dramatically, with a global maximum at low-micromolar dye concentration. In contrast, at high total Trp concentration (1 mM, Fig. 5d) the dye-to-dye collisions are not as important for depletion of the ^{T1}D population. This result stems from the fact that the photo-CIDNP-favoring collision of ^{T1}D with Trp is much more frequent at high total Trp concentration.

When laser-light penetration through the NMR sample is taken into account (long-dashed lines of panels c and d of Fig. 5), it is clear that the population of the ^{T1}D state is much lower, regardless of Trp concentration. This phenomenon is a consequence of the large absorption cross section of FL. To provide a realistic account of our experimental conditions, all the simulations in panels e through h take both collisional quenching and light penetration through the NMR sample into account.

Next, we performed simulations at a low total Trp concentration. As shown in Figure 5e, at the optimized total FL concentration of 3–4 μM (close to the experimentally detected value

of 6 μM), the rate constant k_{TS}, pertaining to the nonradiative processes that decrease the triplet dye (^{T1}D) (and that do not depend on dye-to-dye collisions), has a large influence on the steady-state concentration of ^{T1}D. Hence this rate constant is predicted to be an important parameter for any photo-CIDNP-active dye targeting efficient NMR data collection at low sample concentration. In contrast, at high total Trp concentration (1 mM, see Fig. 5f), it is clear that the k_{TS} rate constant is not a critical parameters, since the triplet dye concentration is only negligibly dependent on the value assigned to k_{TS}.

Panel g of Figure 5 shows a superposition of the simulated and experimental data for photo-CIDNP at 10 μM total Trp (see also Fig. S9). A good agreement between computations and experiments is observed, suggesting that our simulations properly capture the nature of the phenomenon. As shown in Table 1, the experimentally determined known value [36] of k_{TS} for the FL dye is 50 s^{-1}, which is 98-fold smaller than the corresponding value for FMN. The small known value of k_{TS} of FL, together with the simulations in Figure 5e and the generally good agreement between simulated and experimental data in Figure 5g highlight the fact that the long excited-state triplet lifetime of FL is likely an important contributor to the favorable photo-CIDNP behavior of this dye.

Next, we estimated the predicted dependence of the steady-state triplet dye concentration on electron-transfer rate. Electron transfer is a key process in photo-CIDNP that takes place after the dye and the NMR-active molecule of interest have formed the collision complex denoted in Figure 5a as (^{T1}D Trp). While an experimental value for the electron-transfer rate constants ket for the oxidation of Trp by triplet excited-state FL is not currently available, we predicted this value according to Marcus electron transfer theory [37,38,39] applied to the Trp-FL collision complex, upon taking into account a number of experimentally available parameters, including the $T_1 \rightarrow S_0$ energy gap of FL (see Table 1). The simulations in panels c-f of Figure 5 use this value. In panel h of Figure 5, we estimated how the steady-state FL triplet dye concentration is expected to depend on the electron transfer rate constant k_{et}. Interestingly, this dependence is found to be rather steep. This result is important because it shows that, in addition to a small k_{TS} value and a high extinction coefficient, photo-CIDNP experiments also benefit from a large electron-transfer rate constant. While high electron-transfer rates depopulate the triplet excited-state dye, they favor radical-pair formation, a key intermediate in photo-CIDNP.

We then estimated the expected total ^{T1}D concentration as a function of extinction coefficient (ε) of the dye (^{So}D). The ε parameter plays an important role in modulating the ^{T1}D concentration upon laser irradiation. This concept is best appreciated upon close inspection of the kinetic scheme in Figure 5a. This scheme shows that a high value of ε is expected to shift the $^{So}D \rightarrow {}^{S1}D$ reaction to the right, at any given total dye concentration. In addition, a high dye concentration increases the rate of the self-quenching ($^{T1}D + {}^{So}D \rightarrow 2\ {}^{So}D$) process, which depopulates ^{T1}D. Hence, low ^{So}D dye concentrations seem to be generally desirable. Now, our kinetic simulations show that at low Trp concentration higher values of the extinction coefficient ε promote higher values of the maximum achievable steady-state ^{T1}D (Fig. 6 a and b). In contrast, at high Trp concentration the value of ε has a much smaller effect on the maximum achievable ^{T1}D (Fig. 6c). Hence, it is clear that dyes with high ε values are expected to be highly beneficial at low Trp concentration because they

enable achieving large ^{T1}D concentration while keeping the total ^{So}D concentration low. In this way, the contribution of unproductive self-quenching pathways is minimized. A graphical representation of this overarching conclusion is provided in the bar graph of Figure 6d.

In summary, the synergistic analysis of kinetic simulations and experiments lead to the following take-home messages regarding FL's peculiar behavior as a photo-CIDNP sensitizer. At first glance, inspection of Table 1 may erroneously suggest that the photophysical properties of FL, particularly its slow k_{isc} and fast k_{fl}, qualify it as an unsuitable photo-CIDNP dye. Importantly however, our kinetic simulations and experiments showed that, at extremely low concentration of the NMR-active molecule of interest (e.g., Trp or Tyr at ca. 1–10 μM), the long triplet-state lifetime (k_{TS}^{-1}) and the high extinction coefficient (ε) of FL override the unfavorable small k_{isc} and large k_{fl} values and contribute to render FL an excellent photo-CIDNP sensitizer. Best results are obtained when the total FL concentration ($[D]_{TOT}$ in Figs. 5 and 6) is optimized for each concentration of the NMR-active molecule of interest. Optimal FL concentrations are usually in the low micromolar range. Finally, the kinetic simulations of Figure 5h suggest that future experimental determinations and optimization of electron transfer rates have the potential to further improve FL's efficiency as a photo-CIDNP sensitizer.

The extent of potential photo-damage of FL and Trp induced by laser irradiation was explicitly tested following photo-CIDNP long-term data collection. We found that at low μM Trp and FL concentration only a moderate extent of inactivation of each species occurs, amounting to approximately 0.5 % per scan (Supplementary Fig. S5). The cumulative S/N of Trp keeps increasing steadily even after 80 scans. This result confirms that the FL photo-CIDNP sensitizer is compatible with long-term NMR data collection. Therefore, while it is generally preferable to collect as few scans as possible for overall minimization of photodamage, several transients can be acquired with negligible consequences for sample integrity at 1–5 μM Trp. More detailed comments on photoinduced inactivation are provided in the Supporting Information.

Conclusions

In summary, this study shows that fluorescein is an excellent photo-CIDNP sensitizer suitable for hypersensitive NMR data collection in liquids down to an unprecedented 1 μM concentration. The experiments shown here lead up to two-thousand-fold time savings relative to the best non-photo-CIDNP state-of-the-art setups. Future investigations will test the applicability of this methodology to a wider array of biomolecules. More detailed future mechanistic studies involving time-resolved photo-CIDNP experiments employing pulsed lasers will be instrumental to reveal the contribution of F-pairs and degenerate electron exchange polarization effects to photo-CIDNP at low sample concentration in the presence of FL.

It is worth noticing that SABRE, an alternative hyperpolarization method applicable to the liquid state[10], recently enabled prompt data collection down to 500 nanomolar. However,

unlike SABRE, photo-CIDNP has a wider range of applicability to diverse substrates, including a variety amino acids, polypeptides and proteins[26,29,30,40].

Supplementary Material

Refer to Web version on PubMed Central for supplementary material.

Acknowledgments

We thank Charlie Fry, Lingchao Zhu and Marco Tonelli for technical assistance. We are also grateful to Jung Ho Lee and Heejun Choi for helpful discussions. This research was funded by the National Institutes of Health (grant 1R21GM111611) and University of Wisconsin–Madison Bridge Funds from the College of Letters and Sciences. This study made use of the National Magnetic Resonance Facility at Madison, which is supported by NIH grant P41GM103399 (NIGMS), old number: P41RR002301. Equipment was purchased with funds from the University of Wisconsin-Madison, the NIH P41GM103399, S10RR02781, S10RR08438, S10RR023438, S10RR025062, S10RR029220), the NSF (DMB-8415048, OIA-9977486, BIR-9214394), and the USDA.

References

1. Lepre CA, Moore JM, Peng JW. Theory and Applications of NMR-Based Screening in Pharmaceutical Research. Chem. Rev. 2004; 104:3641–3676. [PubMed: 15303832]
2. Saalwächter K. Proton Multiple-Quantum NMR for the Study of Chain Dynamics and Structural Constraints in Polymeric Soft Materials. Prog. Nucl. Magn. Reson. Spectrosc. 2007; 51:1–35.
3. Kay LE. NMR Studies of Protein Structure and Dynamics. J. Magn. Reson. 2005; 173:193–207. [PubMed: 15780912]
4. Preston CM. Applications of NMR to Soil Organic Matter Analysis: History and Prospects. Soil Sci. 1996; 161:144–166.
5. Griesinger C, Bennati M, Vieth HM, Luchinat C, Parigi G, Hofer P, Engelke F, Glaser SJ, Denysenkov V, Prisner TF. Dynamic Nuclear Polarization at High Magnetic Fields in Liquids. Prog. Nucl. Magn. Reson. Spectrosc. 2012; 64:4–28. [PubMed: 22578315]
6. Günther, UL. Modern NMR Methodology. Springer; 2013. p. 23-69.
7. Lee JH, Okuno Y, Cavagnero S. Sensitivity Enhancement in Solution NMR: Emerging Ideas and New Frontiers. J. Magn. Reson. 2014; 241:18–31. [PubMed: 24656077]
8. Ardenkjaer-Larsen JH, Fridlund B, Gram A, Hansson G, Hansson L, Lerche MH, Servin R, Thaning M, Golman K. Increase in Signal-to-Noise Ratio of > 10,000 Times in Liquid-State NMR. Proc. Natl. Acad. Sci. U. S. A. 2003; 100:10158–10163. [PubMed: 12930897]
9. Natterer J, Bargon J. Parahydrogen Induced Polarization. Prog. Nucl. Magn. Reson. Spectrosc. 1997; 31:293–315.
10. Eshuis N, Hermkens N, van Weerdenburg BJ, Feiters MC, Rutjes FP, Wijmenga SS, Tessari M. Toward Nanomolar Detection by NMR through Sabre Hyperpolarization. J. Am. Chem. Soc. 2014; 136:2695–2698. [PubMed: 24475903]
11. Adams RW, Aguilar JA, Atkinson KD, Cowley MJ, Elliott PIP, Duckett SB, Green GGR, Khazal IG, López-Serrano J, Williamson DC. Reversible Interactions with Para-Hydrogen Enhance NMR Sensitivity by Polarization Transfer. Science. 2009; 323:1708–1711. [PubMed: 19325111]
12. Navon G, Song Y, Room T, Appelt S, Taylor RE, Pines A. Enhancement of Solution NMR and Mri with Laser-Polarized Xenon. Science. 1996; 271:1848–1848.
13. Walker TG, Happer W. Spin-Exchange Optical Pumping of Noble-Gas Nuclei. Reviews of Modern Physics. 1997; 69:629–642.
14. Haupt J. A New Effect of Dynamic Polarization in a Solid Obtained by Rapid Change of Temperature. Phys. Lett. A. 1972; 38:389–390.
15. Carver TR, Slichter CP. Polarization of Nuclear Spins in Metals. Physical Review. 1953; 92:212–213.
16. Bargon J, Fischer H, Johnson U. Nuclear Magnetic Resonance Emission Lines During Fast Radical Reactions. I. Recording Methods and Examples. Z. Naturforsch. A. 1967; 22:1551–1555.

17. Ward HR, Lawler RG. Nuclear Magnetic Resonance Emission and Enhanced Absorption in Rapid Organometallic Reactions. J. Am. Chem. Soc. 1967; 89:5518–5519.
18. Daviso E, Janssen GJ, Alia A, Jeschke G, Matysik Jr, Tessari M. A 10 000Fold Nuclear Hyperpolarization of a Membrane Protein in the Liquid Phase Via a Solid-State Mechanism. J. Am. Chem. Soc. 2011; 133:16754–16757. [PubMed: 21962225]
19. Goez M, Kuprov I, Hore PJ. Increasing the Sensitivity of Time-Resolved Photo-Cidnp Experiments by Multiple Laser Flashes and Temporary Storage in the Rotating Frame. J. Magn. Reson. 2005; 177:139–145. [PubMed: 16122958]
20. Feldmeier C, Bartling H, Riedle E, Gschwind RM. Led Based NMR Illumination Device for Mechanistic Studies on Photochemical Reactions-Versatile and Simple, yet Surprisingly Powerful. J. Magn. Reson. 2013; 232:39–44. [PubMed: 23685874]
21. Grosse S, Gubaydullin F, Scheelken H, Vieth H-M, Yurkovskaya A. Field Cycling by Fast NMR Probe Transfer: Design and Application in Field-Dependent Cidnp Experiments. Appl. Magn. Reson. 1999; 17:211–225.
22. Lee JH, Cavagnero S. A Novel Tri-Enzyme System in Combination with Laser-Driven NMR Enables Efficient Nuclear Polarization of Biomolecules in Solution. J. Phys. Chem. B. 2013; 117:6069–6081. [PubMed: 23560683]
23. Lee JH, Sekhar A, Cavagnero S. 1h–Detected 13c Photo-Cidnp as a Sensitivity Enhancement Tool in Solution NMR. J. Am. Chem. Soc. 2011; 133:8062–8065. [PubMed: 21548581]
24. Sekhar A, Cavagnero S. Epic- and Chance-Hsqc: Two 15n Photo-Cidnp-Enhanced Pulse Sequences for the Sensitive Detection of Solvent-Exposed Tryptophan. J. Magn. Reson. 2009; 200:207–213. [PubMed: 19643649]
25. Goez, M. Annual Reports on NMR Spectroscopy. Webb, GA., editor. Vol. 66. London: Academic Press; 2009. p. 77-147.
26. Hore PJ, Broadhurst RW. Photo-Cidnp of Biopolymers. Prog. Nucl. Magn. Reson. Spectrosc. 1993; 25:345–402.
27. Zysmilich MG, McDermott A. Photochemically Induced Dynamic Nuclear Polarization in the Solid-State 15n Spectra of Reaction Centers from Photosynthetic Bacteria Rhodobacter Sphaeroides R-26. J. Am. Chem. Soc. 1994; 116:8362–8363.
28. Prakash S, Gast P, Alia, de Groot HJ, Matysik J, Jeschke G. Photo-Cidnp Mas NMR in Intact Cells of Rhodobacter Sphaeroides R26: Molecular and Atomic Resolution at Nanomolar Concentration. J. Am. Chem. Soc. 2006; 128:12794–12799. [PubMed: 17002374]
29. Kaptein R, Dijkstra K, Nicolay K. Laser Photo-Cidnp as a Surface Probe for Proteins in Solution. Nature. 1978; 274:293–294. [PubMed: 683312]
30. Kuhn, LT. Hyperpolarization Methods in NMR Spectroscopy. Springer: 2013. p. 229-300.
31. Muszkat KA. Photo-Cidnp in the Tyrosyl Unit: A New Tool in High Resolution Nuclear Magnetic Resonance Studies of Peptides. J. Chem. Soc., Chem. Commun. 1977:872–873.
32. Muszkat K, Gilon C. Cidnp in Tyrosyl Protons of Luliberin. Nature. 1978
33. Fasman, GD.; Sober, HA. Handbook of Biochemistry and Molecular Biology. Vol. 4. CRC press Cleveland; 1977.
34. Song L, Hennink E, Young IT, Tanke HJ. Photobleaching Kinetics of Fluorescein in Quantitative Fluorescence Microscopy. Biophys. J. 1995; 68:2588. [PubMed: 7647262]
35. Kay L, Keifer P, Saarinen T. Pure Absorption Gradient Enhanced Heteronuclear Single Quantum Correlation Spectroscopy with Improved Sensitivity. J. Am. Chem. Soc. 1992; 114:10663–10665.
36. Lindqvist, L. A Flash Photolysis Study of Fluorescein. Vol. 16. Almqvist & Wiksell; 1960.
37. Marcus RA. On the Theory of Oxidation-Reduction Reactions Involving Electron Transfer. I. J. Chem. Phys. 1956; 24:966–978.
38. Marcus RA. Electron Transfer Reactions in Chemistry. Theory and Experiment. Reviews of Modern Physics. 1993; 65:599.
39. Marcus RA, Sutin N. Electron Transfers in Chemistry and Biology. Biochim. Biophys. Acta. 1985; 811:265–322.

40. Mok KH, Kuhn LT, Goez M, Day IJ, Lin JC, Andersen NH, Hore PJ. A Pre-Existing Hydrophobic Collapse in the Unfolded State of an Ultrafast Folding Protein. Nature. 2007; 447:106–109. [PubMed: 17429353]

41. Fritz B, Matsui K, Kasai S, Yoshimura A. Triplet Lifetimes of Some Flavins. Photochem. Photobiol. 1987; 45:539–541.

42. Vaish SP, Tollin G. Flash Photolysis of Flavins. Iv. Some Properties of the Lumiflavin Triplet State. J. Bioenerg. 1970; 1:181–192. [PubMed: 5005954]

43. Sjöback R, Nygren J, Kubista M. Absorption and Fluorescence Properties of Fluorescein. Spectrochimica Acta Part A. 1995; 51:L7–L21.

44. Chambers RW, Kearns DR. Triplet States of Some Common Photosensitizing Dyes. Photochem. Photobiol. 1969; 10:215–219. [PubMed: 5824756]

45. Tsentalovich YP, Lopez J, Hore P, Sagdeev R. Mechanisms of Reactions of Flavin Mononucleotide Triplet with Aromatic Amino Acids. Spectrochim. Acta A. 2002; 58:2043–2050.

46. Togashi DM, Szczupak B, Ryder AG, Calvet A, O'Loughlin M. Investigating Tryptophan Quenching of Fluorescein Fluorescence under Protolytic Equilibrium. J. Phys. Chem. A. 2009; 113:2757–2767. [PubMed: 19254018]

47. Okuda M, Momose Y, Niizuma S, Koizumi M. Esr Studies on the Behavior of Fluorescein Semiquinone. Bull. Chem. Soc. Jpn. 1967; 40:1332–1338.

48. Kaptein R. Simple Rules for Chemically Induced Dynamic Nuclear Polarization. J. Chem. Soc., Chem. Commun. 1971:732–733.

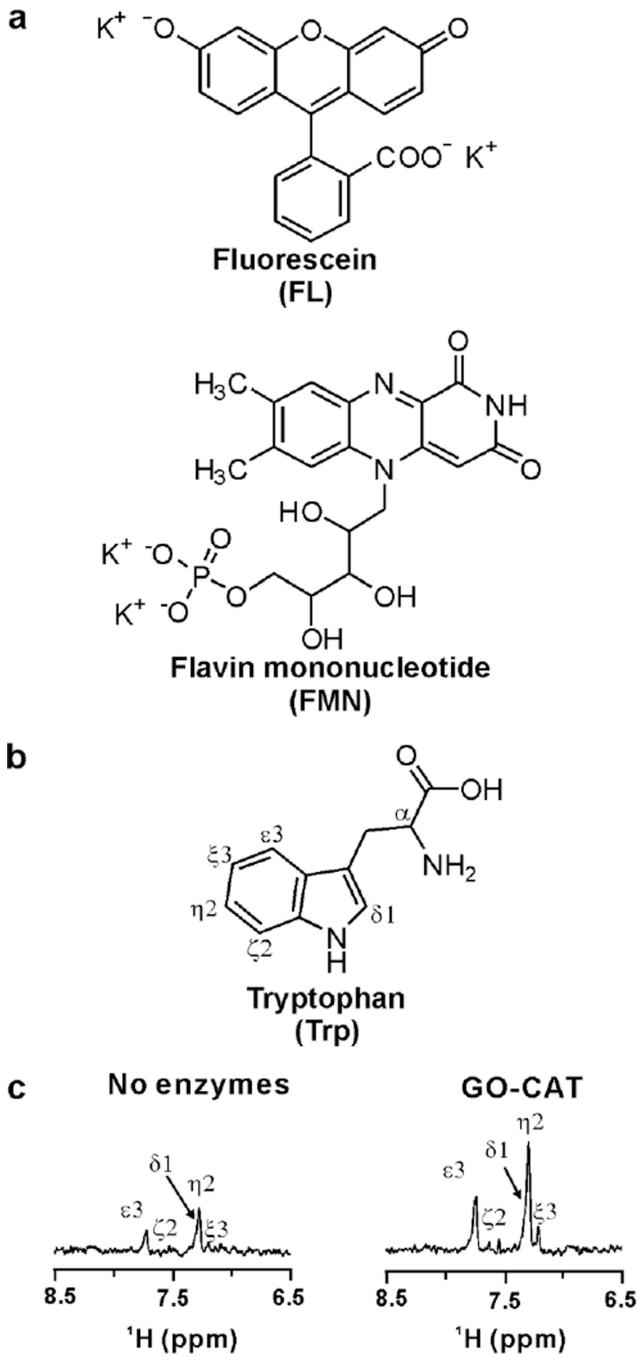

Figure 1.

(a) Structure of flavin mononucleotide (FMN) and fluorescein (FL), the two photosensitizers employed in this work. (b) Structure of tryptophan (Trp). (c) 1D ^{13}C PRINT photo-CIDNP NMR spectra of 1 mM Trp (30 μM FL, in 10 mM K^+ phosphate, 5% D_2O, pH 7.0, 25 °C) in the absence and presence of catalytic amounts of the GO-CAT enzyme system (see Experimental Methods). A single scan was acquired in both experiments (argon-ion laser in multiline mode, 1.5 W and 0.1 s irradiation time, Varian Inova 600 MHz NMR spectrometer equipped with a room-temperature probe).

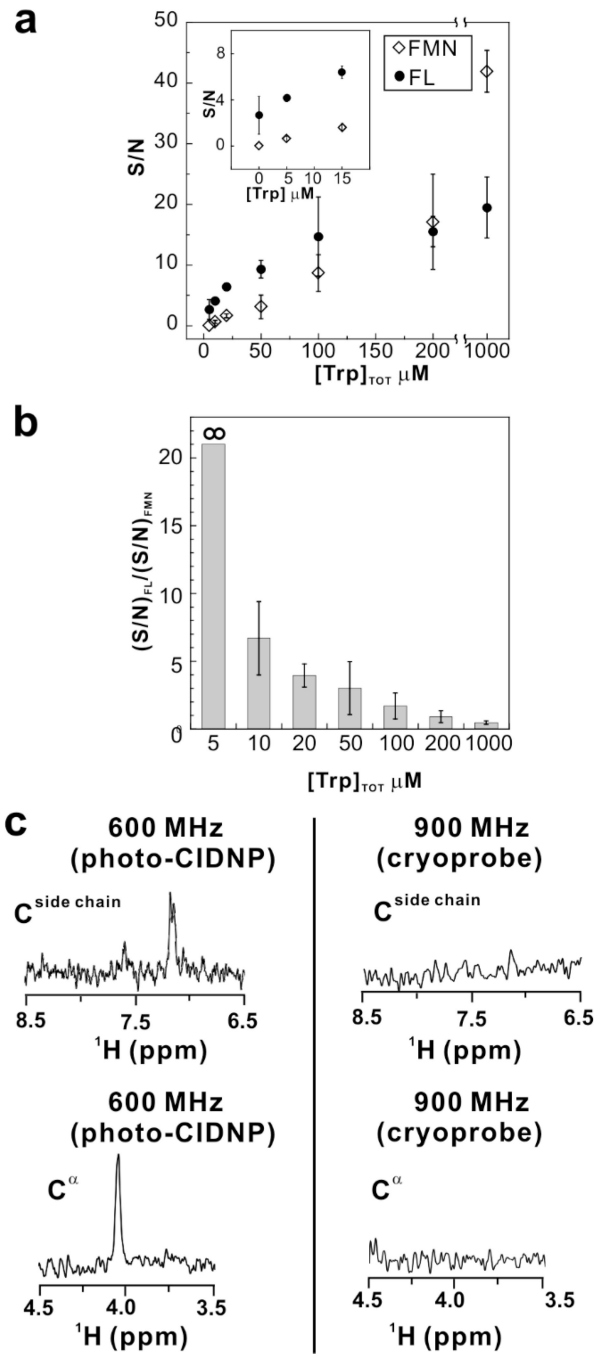

Figure 2.

(a) Concentration dependence of Trp S/N for the $^{1}H^{\eta 2}$ resonance in a ^{13}C PRINT photo-CIDNP NMR experiment. Data were collected in the presence of catalytic amounts of the oxygen-scavenging GO-CAT enzymes (see Experimental Methods) and either the FL or FMN photosensitizers. Sample conditions and data acquisition parameters were as in Fig. 1 except that photosensitizer dye concentrations were individually optimized at each Trp concentration (optimized FL and FMN concentrations ranged from 6 to 30 μM and from 3 to 200 μM, respectively). No signal was observed for 5 μM Trp at any FMN concentration.

Two-to-six experiments were performed for each data point. Uncertainties were expressed as ± one standard error. (b) Bar graph illustrating the ratio of the photo-CIDNP signal-to-noise values in panel a, employing either FL or FMN as photosensitizers. (c) ^{13}C PRINT photo-CIDNP NMR spectra of aromatic side-chain and C^{α} resonances of 5 μM Trp in the presence of 6 μM FL. Data were collected at 14.1 Tesla (a 600 MHz NMR spectrometer). All other sample conditions and data collection parameters were as in (a), except that 8 scans were acquired (relaxation delay: 2.5 s). For comparison, sensitivity-enhanced ^{1}H-^{13}C HSQC (SE-HSQC) spectra are also shown, with data collected on a 900 MHz NMR spectrometer equipped with a cryogenic probe (8 scans, relaxation delay 2.5 s).

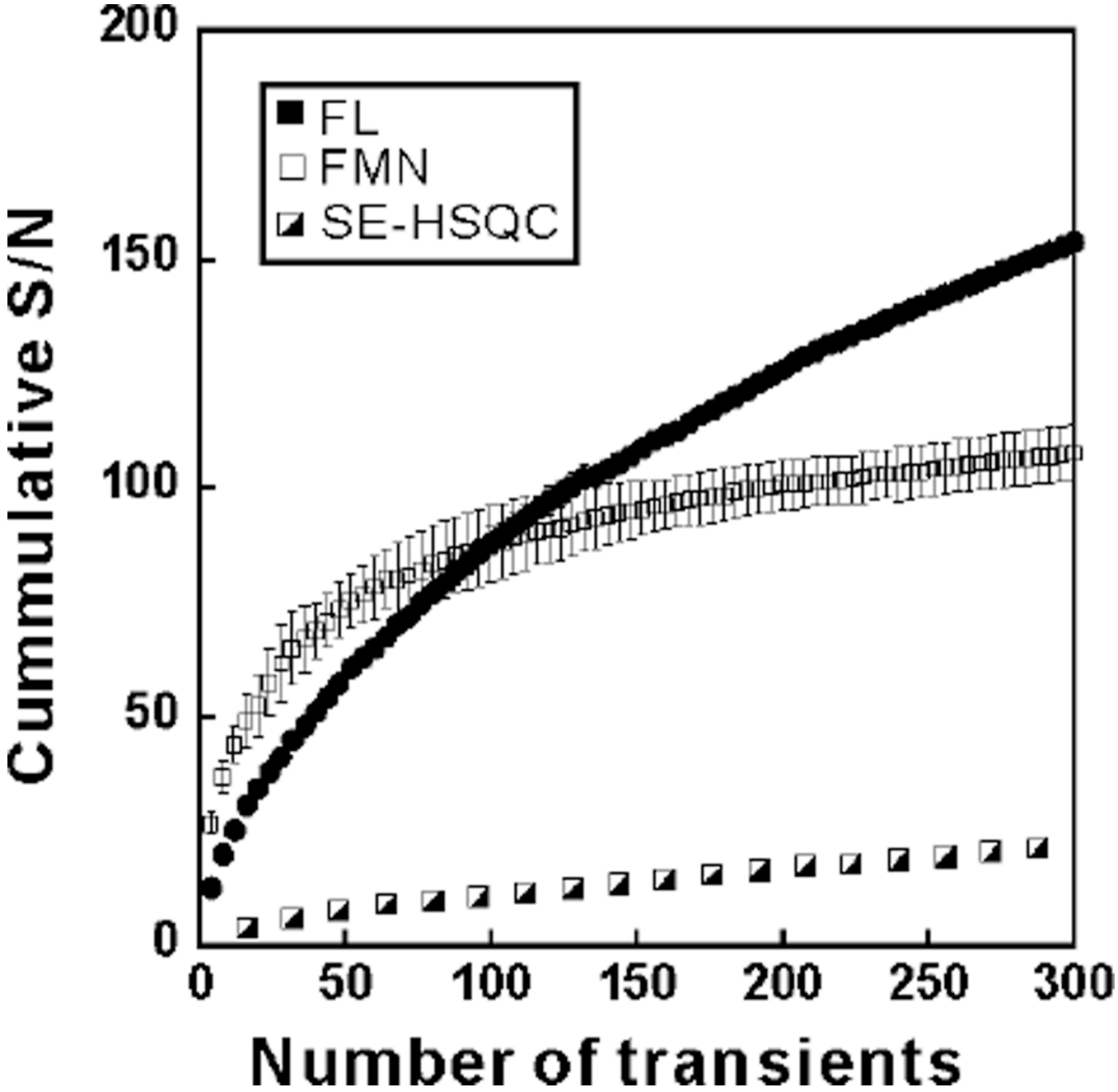

Figure 3.

Long-term photo-CIDNP NMR data collection in the presence of FL and FMN. Cumulative signal-to-noise ratio of 200 μM Trp ($^{1}H^{\eta 2}$ resonance) in a ^{13}C PRINT photo-CIDNP experiment (argon-ion laser in multiline mode, 0.5 Watt laser irradiation power, 0.1s irradiation time) upon long-term data collection. Either 60 μM total FL or 200 μM total FMN were used. All experiments included catalytic amounts of the GO and CAT enzymes (see Experimental Methods for details). The experiments with FMN also included catalytic amounts of the NR enzyme (0.3 units). All other sample conditions and data acquisition parameters were as in the legend of Figure 1. Seventy-five successive data sets, comprising 4

scans each, were collected and cumulative signal-to-noise was calculated according to eq. (2). Three-to-four experiments were performed for each data point. Uncertainties are expressed as ± one standard error.

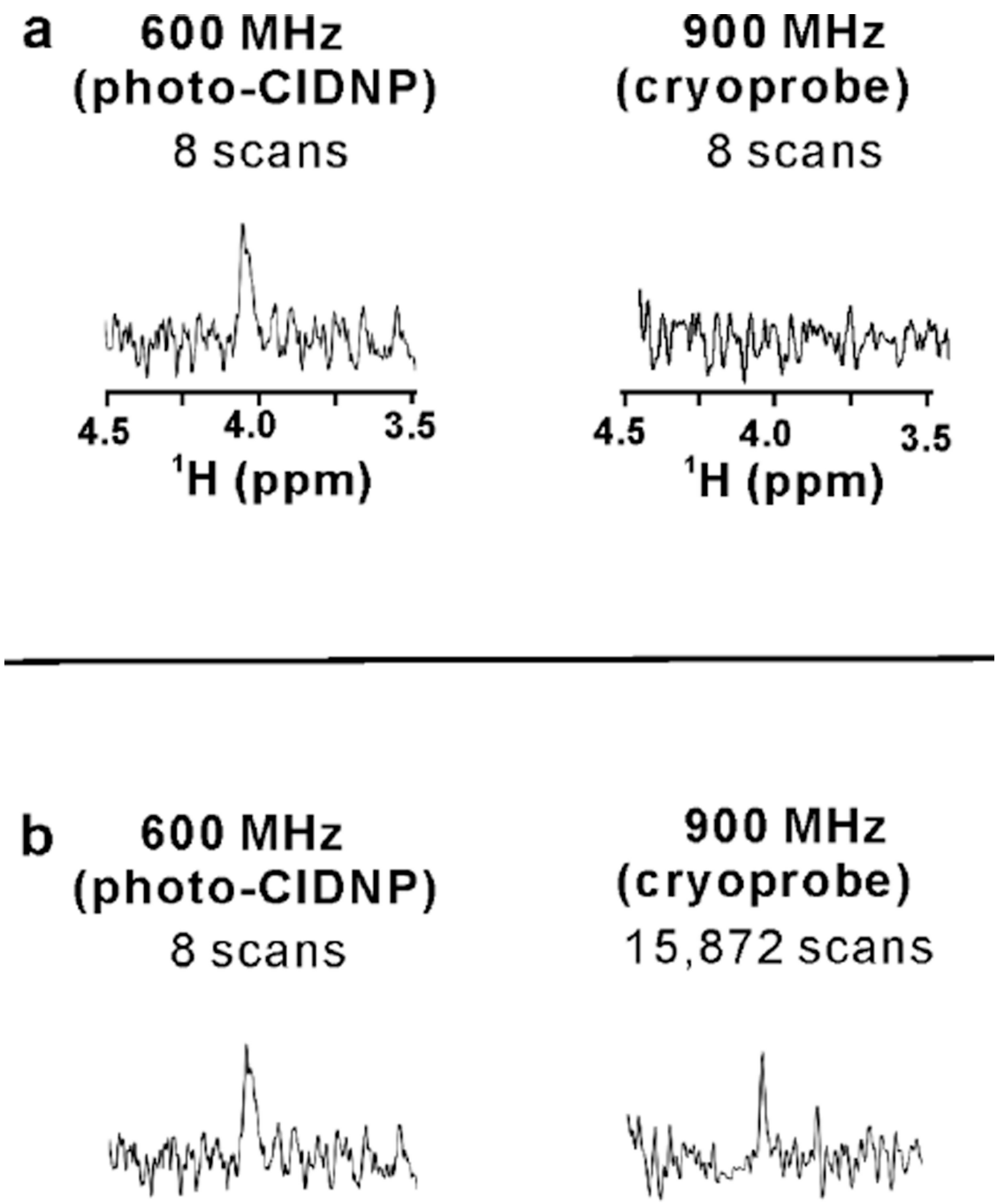

Figure 4.

Photo-CIDNP NMR capability to perform rapid analysis of 1 μM Trp in solution. (a) NMR spectra of 1 μM Trp (solution conditions as in the legend of Fig. 1, H^{α} resonance, 2.4 μM FL, 8 scans) collected either at 14.1 Tesla (600 MHz) with a room-temperature probe in the presence of photo-CIDNP (1D ^{13}C PRINT), or at 21.2 Tesla (900 MHz) with a cryogenic probe (^{1}H-^{13}C SE-HSQC) in the absence of photo-CIDNP. (b) Same experiments as in panel a except that extensive signal averaging (15,872 scans) was carried out at 21.2 Tesla, until

the S/N of the experiment at 21.2 Tesla became approximately the same as the S/N of the experiment at 14.1 Tesla.

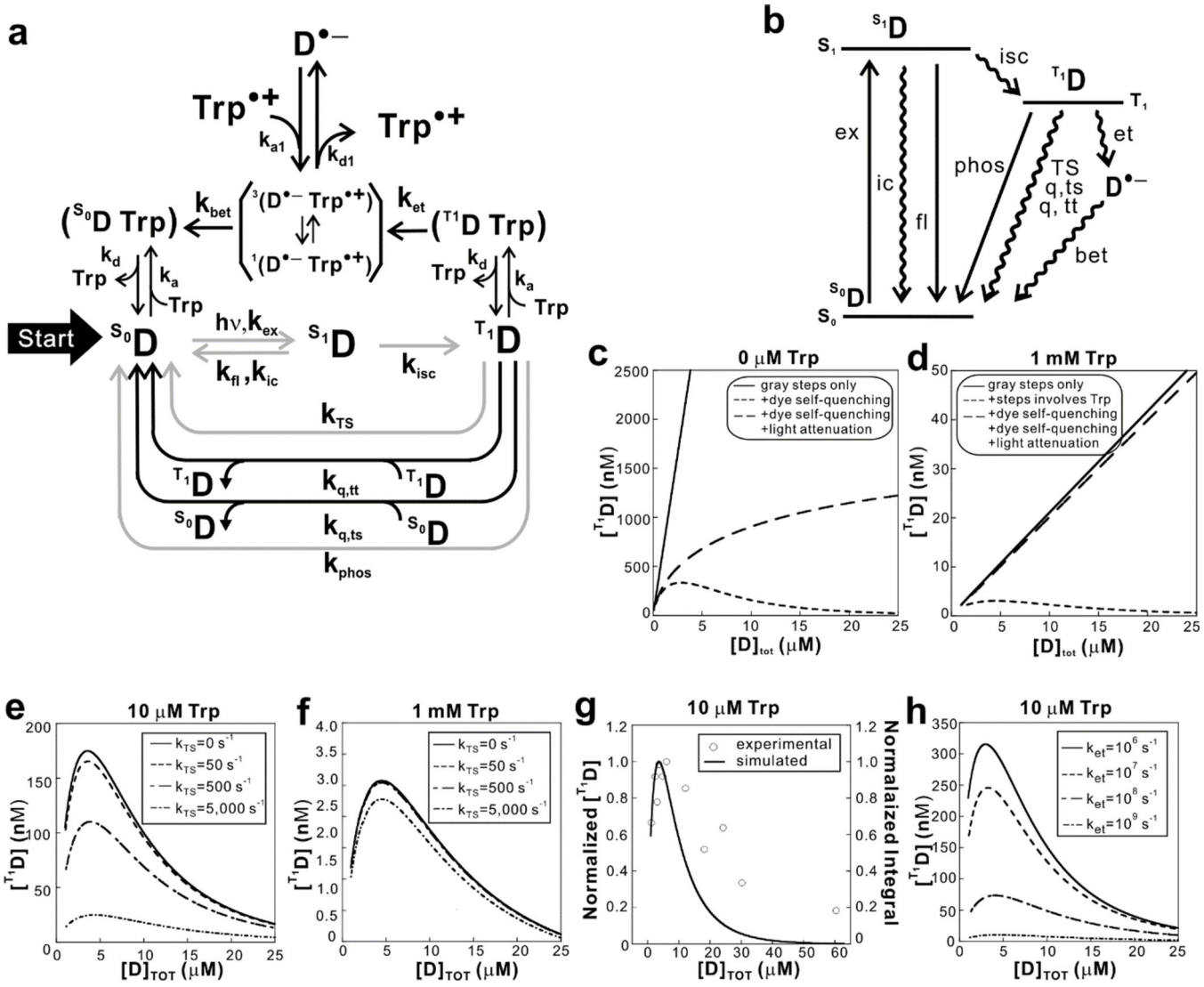

Figure 5.

Kinetic simulations of processes involving photo-CIDNP dyes. (a) Scheme illustrating the kinetic model used in the simulations, D denotes the photo-CIDNP dye. The notations for each process and rate constant definitions are the same as in Table 1. Although spin-multiplicities of the radical ion pairs are not explicitly included in this scheme, the actual kinetic simulations explicitly involved the treatment of each of the three triplet radical ion pairs (see Supporting Information). (b) Energy diagram summarizing the salient processes governing the fate of the FL dye upon photoexcitation. (c) Simulated steady-state photoexcited triplet dye (^{T1}D) concentration as a function of total dye concentration ([D] $_{TOT}$) at infinitely low NMR-sample concentration ([Trp] $\rightarrow$ 0). The gray steps listed in the legend refer to the gray steps in panel a. (d) analogous simulation to the one reported in panel c except that the simulated total Trp concentration is 1 mM. (e) Simulated dependence of the steady-state [^{T1}D] on [D] $_{TOT}$ for different values of the non-radiative triplet-to-singlet decay rate constants at 10 μM total Trp concentration. (f) same as panel e except that the simulated total Trp concentration was 1 mM. (g) Experimentally determined photo-CIDNP

NMR signal-to-noise ratio (open circles, data acquisition parameters as in Fig. 2) and computed (black line) steady-state ^{T1}D concentration plotted as a function of $[D]_{TOT}$ Experimental and computed data were normalized so that the maximum value of each is equal to 1. Single experiment was performed except data point at 1.2 and 6 μM of total FL. Uncertainties were expressed as ± one standard error. (h) Simulated dependence of the steady-state $[^{T1}D]$ on $[D]_{TOT}$ for different values of the electron transfer rate constant k_{et} at 10 μM total Trp. All simulations in panels e-h take into account the laser-light attenuation upon passage through the NMR sample.

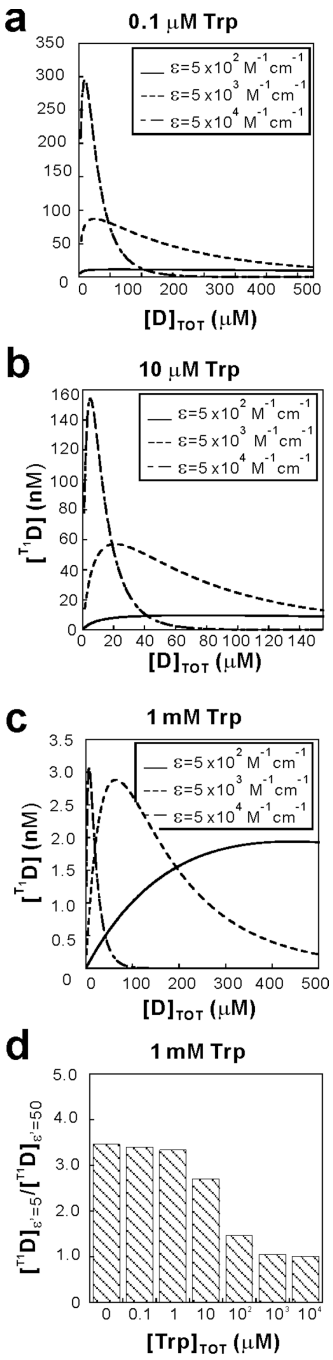

Figure 6.

Kinetic simulations highlighting the role of the dye extinction coefficient ε at variable Trp concentrations. The plots illustrate how the simulated steady-state photoexcited triplet dye (^{T1}D) concentration varies as a function of total dye concentration ($[D]_{TOT}$) for different values of ε, at (a) 0.1 μM, (b) 10 μM and (c) 1 mM total Trp concentration. (d) Simulated ratio of maximal achievable ^{T1}D steady-state concentration using different values of the modified extinction coefficient ε' (ε'=5 and ε'=50) as a function of Trp concentration, where

ε’ denotes the extinction coefficient in units of 1,000 $M^{-1}cm^{-1}$. See Supporting Information for additional details on the simulations.

Table 1

Selected photophysical properties of FL and FMN.

	FL	Ref.	FMN	Ref.
Intersystem crossing rate constant (k_{isc}) $^{S1}D \rightarrow ^{T1}D$, k_{isc}	3.74×10^6 s^{-1}	34	1.3×10^8 s^{-1}	22
Singlet decay rate constant ($k_{fl}+k_{ic}$) $^{S1}D \rightarrow ^{So}D$	2.134×10^8 s^{-1}	34	8.7×10^7 s^{-1}	22
Triplet decay rate constant (k_{TS})[a] $^{T1}D \rightarrow ^{So}D$	50 s^{-1}	36	4900 s^{-1}	41
Triplet-triplet annihilation rate constant ($kq_{,tt}$) $^{T1}D + {}^{T1}D \rightarrow ^{So}D + {}^{T1}D$	5×10^8 $M^{-1}s^{-1}$	34	8.9×10^8 $M^{-1}s^{-1}$	42
Triplet quenching by ground state rate constant ($kq_{,ts}$) $^{T1}D + {}^{So}D \rightarrow 2\ {}^{So}D$	5×10^7 M^{-1} s^{-1}	34	1.2×10^8 $M^{-1}s^{-1}$	42
Extinction coefficient [b]	76,900 M^{-1} cm^{-1}	43	4,746 M^{-1} cm^{-1}	22
Excitation rate constant (k_{ex}) $^{So}D \rightarrow ^{S1}D$	5,331 s^{-1}	this work[c]	329 s^{-1}	22
$^{So}D \rightarrow ^{T1}D$ energy difference	47.2 kcal	44	50 kcal	45
Observed electron transfer rate constant ($k_{et,obs}$) ^{T1}D +Trp $\rightarrow$RP	NA		1.1×10^9 M^{-1} s^{-1}	45
Trp electron transfer rate constant (k_{et}) (^{T1}D Trp)$\rightarrow$RP	2.91×10^7 s^{-1}	46	NA	
Trp back electron transfer rate constant (k_{bet}) RP$\rightarrow$(^{So}D Trp)	2.27×10^{10} s^{-1}	this work[c]	NA	
Association rate constants involving Trp (k_a) ^{T1}D + Trp$\rightarrow$(^{T1}D Trp) ^{So}D + Trp$\rightarrow$(^{So}D Trp)	7.26×10^9 $M^{-1}s^{-1}$	this work[c]	NA	
Association rate constant involving $Trp^{\bullet+}$ ($k_{a1,TOT}$) $D^{\bullet-}$+$Trp^{\bullet+}$$\rightarrow$RP	1.32×10^{10} $M^{-1}s^{-1}$	this work[c]	NA	
Dissociation rate constant involving Trp (k_d) (^{T1}D Trp) $\rightarrow ^{T1}D$ + Trp (^{So}D Trp) $\rightarrow ^{So}D$ + Trp	4.52×10^9 s^{-1}	this work[c]	NA	
Dissociation rate constant involving $Trp^{\bullet+}$ (k_{d1}) RP$\rightarrow$$D^{\bullet-}$+$Trp^{\bullet+}$	1.52×10^7 s^{-1}	this work[c]	NA	
g factor	2.0034	47	2.0034	48
Triplet-singlet mixing rate constant (k_{mix}) $^{T0}RP \rightarrow ^{S}RP$ $^{S}RP \rightarrow ^{T0}RP$	4.88×10^8 s^{-1}	this work[c]		

[a] Measured at 26 and 25 °C for FMN and FL, respectively.

[b] Measured at 490 and 488 nm for FL and FMN, respectively.

[c] See Supporting Information for details on how this rate constant was estimated.